ChemPubSoc Europe

DOI: 10.1002/chem.201304457

CHEMISTRY A European Journal Full Paper

Magnetic Resonance Imaging

Nanozeolite-LTL with Gd^{III} Deposited in the Large and Eu^{III} in the Small Cavities as a Magnetic Resonance Optical Imaging Probe

Florian Mayer,[a] Wuyuan Zhang,[a] Thomas Brichart,[b] Olivier Tillement,[b] Célia S. Bonnet,[c] Éva Tóth,[c] Joop A. Peters,[a] and Kristina Djanashvili*[a]

Abstract: The immense structural diversity of more than 200 known zeolites is the basis for the wide variety of applications of these fascinating materials ranging from catalysis and molecular filtration to agricultural uses. Despite this versatility, the potential of zeolites in medical imaging has not yet been much exploited. In this work a novel strategy is presented to selectively deposit different ions into distinct framework locations of zeolite-LTL (Linde type L) and it is demonstrated that the carefully ion-exchanged Gd/Eu-containing nanocrystals acquire exceptional magnetic properties in combination with enhanced luminescence. This smart exploitation of the framework structure yields the highest relaxivity density (13.7 $s^{-1} L g^{-1}$ at 60 MHz and 25 °C) reported so far for alumosilicates, rendering these materials promising candidates for the design of dual magnetic resonance/optical imaging probes, as demonstrated in preliminary phantom studies.

Introduction

The alumosilicate frameworks of all zeolites are anionic, due to the presence of tetrahedrally coordinated Al.[1] The negative charges are usually compensated by loosely bound cations, which are accessible for the surrounding solution due to the porous nature of the zeolites. As a result, a fraction of those ions can be easily exchanged by any cation of choice that fits into the pores. In fact, zeolites in which alkali metal ions were exchanged with rare earth ions have been successfully exploited as cracking catalysts in petrochemical processes.[2] The fact that rare earth elements and especially the elements of the lanthanide series are also widely applied in medical imaging, drew the attention of researchers from this field towards zeolites as carriers for paramagnetic Gd^{III} ions applied for contrast enhancement in magnetic resonance imaging (MRI).[3] Such Ln^{III}-loaded zeolite nanoparticles are a versatile tool to overcome sensitivity issues by delivering a high payload of active material with each single particle.[4] Another advantage of the zeolites is that the compartmentalization of their interior can be used to trap ions in different framework environments.[5] This accurate control over the ion locations leads to increased performances of the single components in the zeolite and offers the possibility to combine different imaging modalities in a single probe.[6] Zeolite-LTL (Linde type L) is an interesting candidate for the design of bimodal imaging probes, because it is composed of both large channels that are well accessible for water and smaller cavities that are isolated from the bulk solvent.[5] The framework is built up from so-called cancrinite cages (Figure 1 A), which are connected via their upper and lower six-membered rings to form columns (Figure 1 B, I), interlinked to neighboring columns through oxygen bridges (Figure 1 B, II). This peculiar arrangement creates large channel-like cavities (Figure 1 B, III), which are separated from each other by elliptical eight-membered ring channels (Figure 1 B, IV), parallel to the original columns along the *c*-axis of the crystal. The diameter of the narrowest point of the 12-membered ring "superchannels" (Figure 1 B, III) is 7.1 Å, whereas at the widest point the channel has a free diameter of 12.6 Å (Figure 1 C). Ion exchange in aqueous zeolite-LTL dispersions exclusively takes place in these large channels, as all other cavities are not accessible from the bulk solution.[7] Nevertheless, loading of the other sites can be realized by thermal treatment of the Ln^{III}-exchanged zeolites. The relocation of the large Ln^{III} into the smaller cavities requires high temperatures, and has to be done carefully in order not to destroy the zeolite framework.[5] Ln ions once moved into small cages, are locked there and cannot be exchanged or extracted anymore. In contrast, ions in the largest channels are prone to exchange and 90% of which can be extracted by saturated NH_4Cl aqueous solutions within 24 h.

In this study, Eu^{III} was chosen as an optical reporter because of its sharp emission bands in the visible region (570–720 nm).[8] One of the limiting factors of lanthanides in medical

[a] F. Mayer, W. Zhang, Dr. J. A. Peters, Dr. K. Djanashvili
Department of Biotechnology, Delft University of Technology
Julianalaan 136, 2628 BL Delft (The Netherlands)
Fax: (+31) 152781415
E-mail: k.djanashvili@tudelft.nl

[b] T. Brichart, Prof. O. Tillement
Institut Lumière Materière, Université Claude Bernard Lyon 1
Rue V. Grignard, 69622 Villeurbanne Cedex (France)

[c] Dr. C. S. Bonnet, Dr. É. Tóth
Centre de Biophysique Moleculaire, CNRS
Rue Charles Sadron, 45071 Orleans Cedex 2 (France)

Supporting information for this article is available on the WWW under http://dx.doi.org/10.1002/chem.201304457.

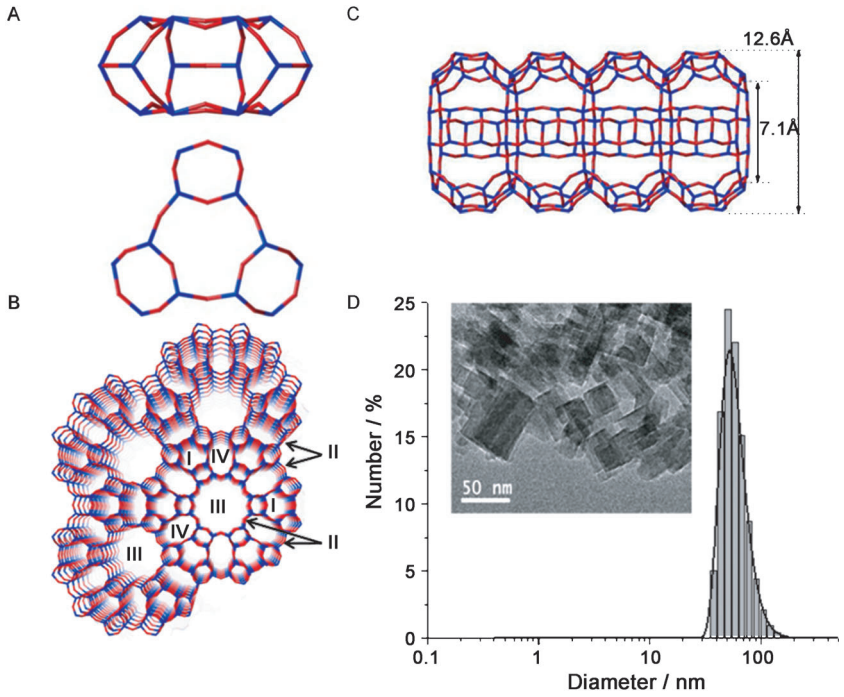

Figure 1. Framework and particle size of zeolite LTL: A) Cancrinite cages (top = view along (100), bottom = view along (001)); B) Detail of the zeolite framework viewed along (001); C) A side view along (100) of the largest channel and its dimensions; D) Hydro-dynamic radius determined by DLS, insert represents a TEM image of zeolite LTL crystals.

imaging is the strong quenching effect of water molecules that are directly coordinated to the luminescent ion. Therefore, we envisioned that the deposition of Eu^{III} in the small cages of the zeolite framework, which are hardly accessible for water molecules, would lead to a dramatic increase of the luminescence intensities and lifetimes. On the other hand, Gd^{III} was chosen as an MRI reporter, since high r_1 relaxivities (increase of the longitudinal water proton relaxation rate in $s^{-1}mM^{-1}$) can be achieved with it.[9] As r_1 is directly proportional to the number of water molecules coordinated to the Gd center (q), loading of Gd^{III} into the big pores of zeolite-LTL pre-loaded with Eu^{III} into the small cages offers an elegant approach for the exploitation of the unique physical properties of each of these lanthanides in combination with the zeolite-LTL framework for the design of a bimodal optical/MRI probe.

Results and Discussion

Loading of zeolite-LTL with lanthanide ions

For the ion exchange, it turned out to be sufficient to stir Na-LTL crystals in an aqueous solution of $LnCl_3$ for 24 h. In this way, loadings up to 5.2 wt% of Ln^{III} into the zeolite (Table 1, Ln-LTL-L) could be achieved. Since only 3.6 alkali ions per unit cell are located in the large channels,[5] the theoretical maximum exchange capacity for Gd^{III} ions is 6.4 wt%. In this context, the achieved 5.2% loading (corresponding to 0.97 Gd^{III} ions per unit cell) is close to complete substitution of the exchangeable alkali ions. The loading did not change substantially upon calcination of the material (Ln-LTL-C), which is not surprising as no ions are extracted during this step and only intra-zeolitic ion migration takes place. To prove this relocation, three different samples were subjected to extensive ion extraction in saturated NH_4Cl solution. The first sample was Gd-loaded (Gd-LTL-L), and the next two were calcined for 6 h at 400 or 600 °C (Gd-LTL-C). Before extraction, all three samples had the same Gd^{III} content

Table 1. Preparation and studies on the properties of double loaded zeolite LTL.

	Ln-LTL-L	Ln-LTL-C[a]	Ln-LTL-E	Ln-LTL-R	Gd-AlTUD1[16a]	Gd-NaY[14]
loading [wt%][b]	5.2 (5.2/0)	5.0 (1.7/3.3)	3.3 (0.0/3.3)	7.9 (4.6/3.3)	3.8	5.0
Si/Al ratio	3	3	3	3	3.5	1.6
q[c]	6.1	6.1/0.9	0.9	6.1/0.9	3.6	7
w[20]	15	32	–	–	94	13
r_1 [$mM^{-1}s^{-1}$][d]	37.8	17.8	8.9	43.8[e]	30.0	12.0
r_1' [$g^{-1}Ls^{-1}$][d]	12.5	5.7	1.9	13.7[e]	7.3	3.8
τ_m [ns]	0.19	–	1660	–	0.27	625
τ_{zeo}[μs]	0.01	–	0.01	–	< 10	33
τ_v [ps]	26.0	–	9.2	–	48	22
Δ^2 [10^{19} s^2]	3.8	–	2.9	–	1.2	5.1
$\ln 1/T_{2e}$[s^{-1}][f]	22.1	22.2	–	–	22.30	22.64
$\ln 1/T_{2e}$[s^{-1}][g]	22.4	21.6	–	–	22.10	22.63
$I_{@615nm}$ (p.d.u.)	120	538	718	415	–	–

[a] 6 h at 600 °C. [b] Total lanthanide loading, between brackets the ratio Gd/Eu determined by BMS (for Gd-LTL) and by EDX (see Figure S1 in the Supporting Information). [c] Determined by luminescence decay of Eu-LTL. [d] 60 MHz, 25 °C. [e] Eu in the small, Gd in the big cavities; [f] Determined from EPR line widths at 0.34 T. [g] Calculated with best fit parameters.

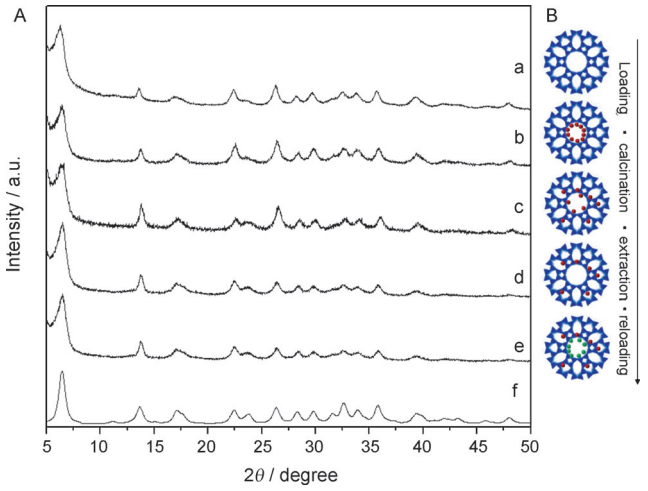

Figure 2. A) XRD patterns of the zeolite framework after different steps of the loading procedure (shown schematically in B). a) initial material (K-LTL), b) after loading with Ln^{III} ions (Ln-LTL-L), c) calcination at 600 °C (Ln-LTL-C), d) extraction of the Ln(red)-ions remaining in the supercage (Ln-LTL-E), and e) reloading of the LTL with Ln(green)-ions (Ln-LTL-R). The last diffractogram f) represents the powder pattern as it was calculated from the database of zeolite structures for the Linde Type L framework with a wavelength of 1.78897 Å ($Co_{K\alpha}$) and $U = 0.5$ for the peak width adjustment.[1c]

of 5 wt%, but after extracting for 72 h the Gd^{III} loading was determined to be 0.48, 2.29, and 3.30% (Gd-LTL-E), for the three samples respectively, showing that only after calcination a considerable amount of Gd^{III} is retained during the extraction step. The influence of the temperature on the migration of the ions is illustrated by the fact that after an increase of the temperature from 400–600 °C, the amount of the migrated ions increased from 2.3 to 3.3 wt%. A subsequent reloading (analogous to the first loading step) yielded materials in which the Gd^{III} loading was increased by 4.6% (Gd-LTL-R), which is comparable to the first loading step, indicating that in all cases the large cavities are available for reloading. After each step, X-ray diffraction patterns were recorded, to demonstrate the integrity of the zeolite structure (Figure 2). The amount of Gd^{III} present in the zeolite framework after each step was determined by bulk magnetic susceptibility (BMS)[10] measurements on aqueous suspensions. From the mass of the dispersed zeolite, the loading was calculated (Table 1). The loading–relocation–extraction procedure is not limited to Gd^{III}, but was also successfully applied to introduce Eu^{III} to the different framework environments. The harsh conditions needed to extract Ln^{III} ions from the framework indicate the strength of the ion absorption in the zeolite. Under all conditions needed for the here presented investigations, no leaching of Gd^{III} ions could be detected. Additionally, the leaching was investigated within the pH range from 4 to 8, as well as in the presence of phosphate ions (Table S1 in the Supporting Information). Only the value obtained for the sample incubated for 24 h at pH 4 in HCl solution was above the detection limit of 4 μM of the colorimetric assay. Clearly, the feasibility of these materials for medical or biological applications will require a more detailed leaching study under physiological conditions, as well as the decoration of the surface with organic moieties along with a thorough toxicology study.

Luminescence study

Dispersions of Ln-LTL-L, Ln-LTL-C, and Ln-LTL-E (Ln = Eu and Gd) in water were investigated with respect to their photophysical properties. The luminescence intensities for both Gd^{III}- and Eu^{III}-loaded samples increased upon calcination, and even further after the extraction step (Figure 3A and Figure S2 in the Supporting Information). This effect was accompanied by an increase in the luminescence decay lifetime. Both phenomena can be explained by the decrease of the amount of water

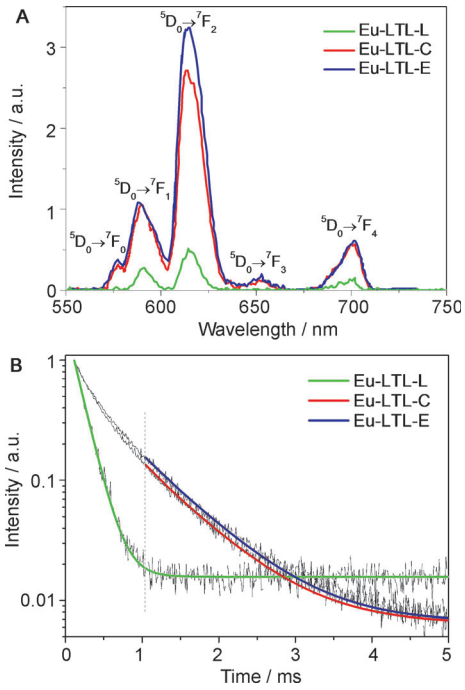

Figure 3. The optical properties of Eu^{III} loaded zeolite LTL. A) Emission spectra of Eu-LTL-L, Eu-LTL-C, and Eu-LTL-E samples obtained in time-resolved mode with a delay of 0.1 ms and an averaging time of 0.1 s. B) Normalized luminescence decay profiles of Eu-LTL-L, Eu-LTL-C, and Eu-LTL-E dispersions, the smooth lines represent the fits that were used to calculate q values, using the data above 1 ms for Eu-LTL-C and Eu-LTL-E.

molecules in the first coordination sphere of the lanthanide ions leading to a reduction of possible nonradiative decay pathways.[11] To get an insight into the different coordination behavior, the luminescence lifetimes were used to determine the number of water molecules in the first coordination sphere of Eu^{III} ions in either location (Figure 3B). From the fitting of the decay curves, the average q values were evaluated to be 6.2, 0.9, and 0.8 for Eu-LTL-L, Eu-LTL-C, and Eu-LTL-E, respectively. To exclude contributions from the fast decaying ions in the large channels, the obtained curves for LTL-C and LTL-E samples were only fitted for lifetimes >1 ms. Thus, the q values reported for those samples only represent the Eu^{III} ions in the small cages. To reproduce the complete decay curves, a bi-exponential fit with one decay constant fixed to the value obtained for Eu-LTL-L (0.158 ms) resulted in functions that fit the whole curve with adjusted R_2 values >0.99 and a second decay constant that was identical with that obtained from the

mono-exponential fit >1 ms. Going from Eu-LTL-C to Eu-LTL-E, the ratios of the pre-exponential factor changed in favor of the longer decaying function, showing that the amount of Eu^{III} ions in the big cage was reduced during the washing procedure.

Relaxivity study and MRI performance

As mentioned above, to optimally exploit the imaging performance of Gd^{III} and Eu^{III} in zeolite-LTL, the latter should be localized in the small cages to reduce the luminescence quenching by water, whereas the MRI performance of Gd^{III} profits from the high q values in the large channels. These effects are illustrated in Figure 4. However, coordinated water is not the only parameter influencing r_1. Other parameters that govern

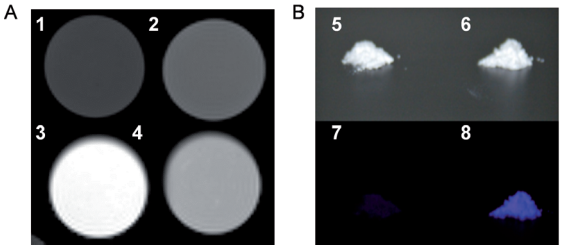

Figure 4. Dual-imaging performance of Gd- and Eu-loaded LTL-zeolite. A) T_1-weighted MR images (7 T, 25 °C) of phantoms formed by four pellets containing 1) 1% aqueous xanthan, 2) Milli-Q water, 3) Gd-LTL-L, and 4) Gd-LTL-E (4) suspended in 1% xanthan at Gd concentration of 0.5 mM; B) Photographic images of solid powders of Eu-LTL-L (5, 7) and Eu-LTL-E (6, 8) under daylight (upper panel) and UV-light of 258 nm (lower panel).

with similar Gd^{III} contents (Figure 5A). The trend of r_1 to decline with the Larmor frequency up to 1 MHz rather than being constant, as usually observed, can be explained by a contribution of the zeolite to the relaxivity due to the long correlation time modulation of the dipole–dipole relaxation of the protons of relatively immobile water molecules adsorbed on the surface of the zeolite particles.[12] Similar phenomena have previously been observed in the NMRD profiles of Gd chelates grafted to hydroxyapatite and TiO_2 particles.[13] By contrast, the low field parts of the NMRD profiles for the Gd-LTL-E are perfectly horizontal. Most likely, the strong adsorption of water to the surface of loaded zeolite particles involves silanol groups, which are removed during calcination. Thus, for the fitting of the obtained ^{1}H NMRD data, a fraction of the silica profile reported by Gillis et al.[12] was subtracted and the magnitude of that fraction was iterated until the low-field part of the resulting profile was horizontal up to a Larmor frequency of about 1 MHz. The resulting profiles are represented in Figure 5B. The local maxima at about 60 MHz in the NMRD profiles of the systems under study are typical for systems with relatively long rotational correlation times (τ_R). Equation (5) (in the Experimental Section) shows that r_1 is proportional to q, which explains the substantial decrease in r_1 upon calcination of Gd-LTL-L. During the calcination, a loss of five water molecules in the first coordination sphere of the Ln^{III} ion occurs. In contrast, r_2 is not depending on q and is similar for Gd-LTL-L and Gd-LTL-E with 93 and 72 $s^{-1}mM^{-1}$ (7 T, 25 °C), respectively. This leads to r_2/r_1 ratios of 3.4 for the loaded versus 22.0 for the extracted material, with the former value being between 1 and 10 as required for optimal performance as positive contrast agents.[3e]

the relaxivity were evaluated by using ^{1}H nuclear magnetic relaxation dispersion (^{1}H NMRD) spectroscopy of aqueous dispersions of Gd-LTL-L and Gd-LTL-E (see Table S2 in the Supporting Information) stabilized with 1% xanthan gum. The ^{1}H NMRD profiles were recorded at different temperatures (Figure S3 in the Supporting Information) from 25 to 50 °C, but for the fittings only the results at 25 °C were used, because at higher temperatures a slight decrease of r_1 was observed over time. A more detailed study (Figure S5 in the Supporting Information) revealed that this effect can be attributed to the presence of xanthan.

The relaxivities of Gd-LTL-L appear to be substantially higher than those of the previously studied Gd^{III}-loaded NaY zeolite

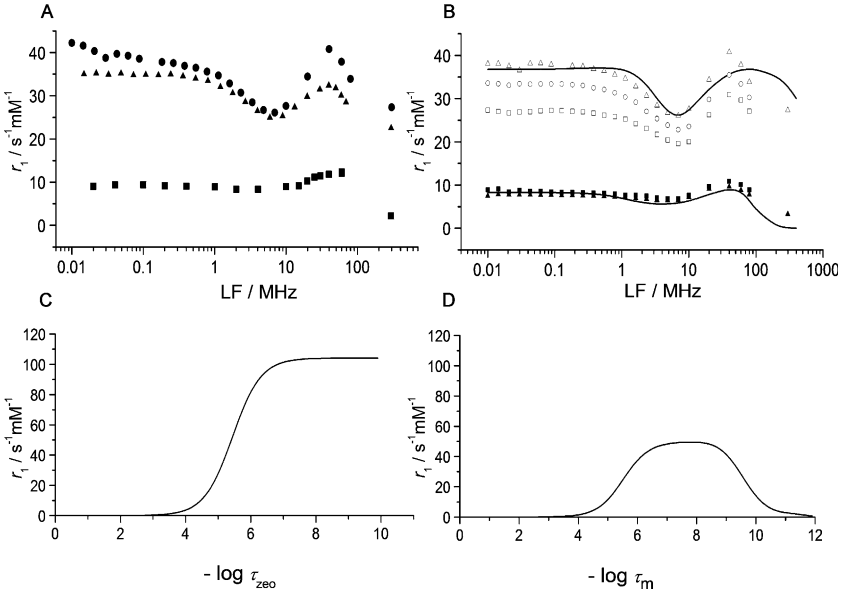

Figure 5. A) ^{1}H NMRD profiles of Gd-LTL-L (●, 5.18% loading, 25 °C), Gd-Al-TUD1 (▲, 3.8% loading, 25 °C)[3e] and Gd-NaY (■, 5% loading, 25 °C).[16a] B) ^{1}H NMRD profiles of the Gd-LTL-L (open symbols) and Gd-LTL-E (filled symbols) at 25 °C (triangles), 37 °C (circles), and 50 °C (squares) after correction for the silica contribution. The curves were calculated with best-fit values, tabulated in Table 1. Simulation of r_1 as a function of C) τ_{zeo} (fixed $\tau_m = 6.5\times10^{-10}$ s) and D) τ_m (fixed $\tau_{zeo} = 6.6\times10^{-8}$ s) using Equations (1)–(5), assuming $\tau_R > 10^{-8}$ s, $\tau_v = 1.4\times10^{-11}$ s, $\Delta^2 = 2.1\times10^{19}$ s^{-2}, $w = 15$,[20] and $q = 6$.

^{1}H NMRD profiles are influenced by a large number of parameters, which makes the quantitative evaluation of these data a difficult task. Therefore, several constraints were introduced. The values of q were fixed at six and one for Gd-LTL-L and Gd-LTL-E, respectively, which are the values determined by the luminescence decay of the corresponding Eu^{III}-loaded samples. As we have demonstrated that for zeolites, r_1 is independent of τ_R implying that $\tau_R \geq 10^{-8}$ s; hence τ_R was fixed to 10^{-8} s.[14] Further constraints could be derived from the peculiar temperature dependence of the relaxivities (Figure 5B), which appears to be opposite for Gd-LTL-L and Gd-LTL-E: for the former, r_1 decreases with temperature, whereas it increases for the latter. The parameters mainly determining the temperature dependence of r_1 are the residence time of the water molecules in the first coordination sphere of Gd^{III} (τ_m) and that of the water molecules inside the zeolite (τ_{zeo}). Evidently, both residence times decrease with increasing temperature meaning that the exchange rates speed up. Two characteristic simulations of the dependence of r_1 on τ_{zeo} and τ_m are displayed in Figure 5C and D. An inspection of these curves shows that the temperature dependencies can only be explained if $\tau_m < 10^{-9}$ s for Gd-LTL-L and $> 10^{-7}$ s for Gd-LTL-E. Furthermore, the decrease of r_1 with temperature for Gd-LTL-L requires that the temperature effect due to τ_{zeo} is small, thus either $\tau_{zeo} > 10^{-4}$ or $< 10^{-8}$ s. The former possibility can be excluded, since that cannot explain the high relaxivities observed for Gd-LTL-L. Based on these considerations τ_{zeo} was fixed at 10^{-8} s and τ_m was constrained to $< 10^{-9}$ s for Gd-LTL-L and to $> 10^{-7}$ s Gd-LTL-E. Finally, further constraints were imposed by performing the fittings of the NMRD profiles simultaneously with EPR line widths (Figure S4 in the Supporting Information) by using a set of equations derived previously.[14] A two-step model was applied taking into account 1) the exchange of Gd^{III}-coordinated water molecules with "free" water molecules inside the zeolite particles and 2) the exchange of "free" water molecules between the outside and inside of the zeolite particles.[14] The details are given in the Experimental Section.

Reasonable fits were obtained, particularly considering the crudeness of the model applied. The best-fit values of the variable parameters are compiled in Table 1 and the NMRD profiles calculated with these values are represented as curves in Figure 5B. The best-fit values of the parameters governing the transversal electronic relaxation rate ($1/T_{2e}$), τ_v and Δ^2, are in the range usually observed for Gd^{III} complexes resulting in values of $1/T_{2e}$ that are in good agreement with the values measured by EPR at 0.34 T (Table 1 and Figure S4 in the Supporting Information). Interestingly, in comparison with reported Gd-NaY, the τ_m of the presented Gd-LTL-L sample is extremely low.[14] The very high water exchange rate between the interior and exterior of Gd-LTL compared to that of Gd-NaY (τ_{zeo} two orders of magnitude smaller) is surprising, since both zeolites have 12-membered ring entrance windows with minimum diameters of 7.1 and 7.4 Å, respectively. Most likely the linear channels are the reason for this fast diffusion within the material. This is corroborated by intracrystalline self-diffusivity measurements by Caro et al., who demonstrated the water mobility in zeolites NaX and NaY with three-dimensional channel structures to be less than that in zeolite ZSM-5 with a linear channel structure.[15] The exchange rate of Gd-LTL is about as fast as for mesoporous materials[16] that have channels with diameters of 1–20 nm. Accordingly, both materials have comparable ^{1}H NMRD profiles with high relaxivities in comparison to the Gd-NaY zeolites (Figure 5A). However, the here presented Gd-LTL material is favorable for application as an MRI contrast agent in contrast to Gd-AlTUD-1, which showed significant leaching of Gd^{III}. It should be noted that relaxivities expressed in $s^{-1}\,mM^{-1}$ do not give a good impression of the efficacy of these materials as MRI contrast agents, due to the difference in loading. Therefore, it is more useful to express them in $s^{-1}\,L\,g^{-1}$ material. Reloaded Gd-LTL-R has a relaxivity density of 13.7 $s^{-1}\,L\,g^{-1}$ at 60 MHz and 25 °C, which is about a factor of two higher than the values for the best zeolitic systems reported up to now (Table 1). This unmatched relaxivity density is also significantly higher than the one of clinically applied Gd^{III}-DOTA (6.6 $s^{-1}\,L\,g^{-1}$ @ 20 MHz, 25 °C).

Conclusion

This work demonstrates interesting photophysical as well as magnetic properties of nanozeolite-LTL acquired upon its loading with Eu^{III} and Gd^{III} ions in the small and big cavities, respectively. The high MRI performance can be explained by the fastest water exchange that was found in zeolitic systems up to now, while the enhanced luminescence could be achieved by the efficient isolation of the Eu^{III} ions from water molecules in the first coordination sphere. Based on these findings, nanozeolite-LTL is an interesting candidate for the development of high performance dual imaging probes, with the potential to be extended for radioisotopes for imaging and/or therapy. However, before the first in vivo studies can be started, more biological tests will be necessary, including cell toxicity and uptake studies. Functionalization of the surface with organic groups will also be investigated to further improve the stability and biocompatibility of this promising system.[17]

Experimental Section

Zeolite loading (Ln-LTL-L)

The obtained K-LTL zeolite was first ion-exchanged with NaCl. This was done in order to obtain Na-LTL, which is supposed to be more active in the ion-exchange with Ln^{III} ions. For this purpose, K-LTL (1 g) was stirred in NaCl solution (20 mL, 1 M) for 20 h. After finishing the exchange, the sample was centrifuged and the solid was washed with water (3×20 mL), re-dispersed in the corresponding Ln-containing solution (15 mL, 80 mM) at pH 5.5, and stirred for 24 h. After this procedure, the dispersion was dialyzed against water (3×1 L). The obtained solution was freeze dried and the resulting powder was collected as Ln-LTL-L sample.

Ion relocation (Ln-LTL-C)

The ion relocation was done in a standard calcination oven. The Ln-LTL-L samples were put in porcelain crucibles and heated to 100 °C at a rate of 1 °C min^{-1} in order to allow the water in the zeolite to escape slowly without damaging the structure. Then the

samples were heated to the desired temperature (400 or 600 °C) at a rate of 10 °C min^{-1}. After reaching the temperature, it was kept constant for 6 h. Then the oven was turned off and left to cool to room temperature. The calcined zeolites were stored in ambient atmosphere for rehydration and they were named Ln-LTL-C.

Extraction (Ln-LTL-E)

Ln-LTL-C samples (1.4 g) were dispersed in saturated aqueous NH_4Cl solution (15 mL). After stirring for 72 h the dispersion was centrifuged and the solid was washed with water (3×20 mL). The re-dispersed sample was then freeze dried to obtain the final Ln-LTL-E product. A detailed investigation indicated that the extraction was already finished after 24 h. Already after this short period more than 90% of the Ln ions were extracted and no change in the following 48 h could be found. This material could be reloaded with another or the same lanthanide according to the above described loading procedure. The NaCl exchange step was not repeated in the second round of loading, because it can be expected that there are only loosely bound NH_4^+ ions present in the channels. The obtained reloaded material was named Ln-LTL-R.

Stability

To investigate the extent of leaching of Gd^{III} ions from the framework, a defined amount of Gd-LTL-L was dispersed in 5 mL of aqueous medium and sonicated for 10 min in an ultrasonic bath. The dispersions were divided into four portions and kept in a thermo-shaker at 37 °C for 24 h. After the incubation time, the zeolite dispersion was centrifuged at 13.2 k rpm and the supernatant was tested for free Gd^{III} ions in a colorimetric assay.[18] Briefly, the supernatant (100 μL) was thoroughly mixed with a freshly prepared acetate buffered xylenol orange solution (1 mL). Then the absorption spectrum was measured in the spectral range from 350 to 600 nm. The ratio of the absorptions at 573 and 433 nm was calculated and used to determine the Gd^{III} concentration by means of a calibration curve, measured in the same way with Gd^{III} stock solutions of known concentrations. The detectable concentrations of Gd^{III} were in a range of 4 to 50 μM with an error of ±2.5 μM. All experiments were repeated in triplicate. The initial Gd^{III} concentration in the Gd-LTL-L dispersions was calculated from the amount of zeolite that was subjected to extraction and the concentration of free Gd^{III} that was found in the supernatant after the extraction.

^{1}H NMRD profiles

For the measurements of the NMRD profiles, defined amounts of loaded and extracted zeolites were dispersed in water containing 1% xanthan gum to stabilize the dispersion for the time of the measurement. Some characteristics of these samples are summarized in Table S2 (in the Supporting Information). Prior to the fitting procedure, the obtained profiles had to be corrected for the contribution of the zeolite framework. Therefore, a fraction of the NMRD profile of pure silica, as it was published by Gillis et al.[12] was subtracted from the obtained data in such a way that the first part of the resulting profile (up to 1 MHz) was constant. The profiles as obtained and after the correction are shown in Figure S3 (in the Supporting Information) and Figure 5 B, respectively. In zeolitic systems studied until now, the diffusion of water from the interior of the zeolite to the bulk limits the relaxivity, and this requires additional parameters to be taken into account for the analysis of the NMRD data. Therefore, we have previously developed a two-step model (Figure S6 in the Supporting Information).[14] First, the relaxivity of the water inside the zeolite nanoparticles (T_{1zeo}) is derived by considering the exchange between water molecules in the first coordination sphere of Gd^{III} and free water molecules inside the zeolite [Eq. (1)]. Here, w is the number of free water molecules (not bound to Gd^{III}) inside the zeolite per Gd^{III} ion and T_{1m} is the longitudinal relaxation time of inner sphere water protons, which is given by the Solomon–Bloembergen–Morgan equation [Eq. (2)].[19]

$$\chi = \frac{1}{T_{1,zeo}} = \frac{\frac{q}{w}}{\tau_m + T_{1m}\left(1+\frac{q}{w}\right)} \quad (1)$$

$$\frac{1}{T_{1m}} = \frac{2}{15}\left(\frac{\mu_0}{4\pi}\right)^2 \frac{\hbar^2\gamma_S^2\gamma_I^2}{r_{GdH}^6} S(S+1)\left(\frac{3\tau_{d1}}{1+\omega_I^2\tau_{d1}^2} + \frac{7\tau_{d2}}{1+\omega_S^2\tau_{d2}^2}\right) \quad (2)$$

Here, r_{GdH} is the effective distance between the Gd^{III} electron spin and the water protons, γ_S and γ_I are the electron and proton gyromagnetic ratios, respectively, and τ_{di} is given by $\tau_{di}^{-1} = \tau_m^{-1} + \tau_R^{-1} + T_{ie}^{-1}$ ($i = 1,2$). The electronic relaxation rates (T_{ie}) are approximated by Equations (3) and (4), in which ω_S is the Larmor frequency, Δ^2 is the trace of the square of the zero field splitting (ZFS) tensor, and τ_v is the correlation time for the modulation of ZFS.

$$\frac{1}{T_{1e}} = 1/25\Delta^2\tau_v[4S(S+1) - 3]\left(\frac{1}{1+\omega_S^2\tau_v^2} + \frac{4}{1+4\omega_S^2\tau_v^2}\right) \quad (3)$$

$$\frac{1}{T_{2e}} = \Delta^2\tau_v\left(\frac{5.26}{1+0.372\omega_S^2\tau_v^2} + \frac{7.18}{1+1.24\omega_S\tau_v}\right) \quad (4)$$

In the second step, the exchange of water between the inside of the zeolite and the bulk by the diffusion through the zeolite channels is considered. This enables the propagation of the relaxation enhancement from the interior of the material to the bulk water outside. If the chemical exchange between protons in two magnetically distinct environments (inside and outside the zeolite) takes place under highly dilute conditions of the paramagnetic entities, Equation (5) can be derived for the overall longitudinal relaxivity.

$$r_1 = \frac{w+q}{55500}\left(\frac{1}{T_{1,zeo}+\tau_{zeo}}\right) \quad (5)$$

Here, τ_{zeo} is the residence lifetime of water protons inside the zeolite. The contribution of water molecules diffusing along the paramagnetic center without being bound to it (the outer sphere contribution) can be neglected for both the exterior and the interior of the investigated materials, because the contribution of this mechanism to the overall relaxivity has been shown to be small for zeolite-immobilized Gd^{III}, particularly at Larmor frequencies higher than 0.1 MHz. This model has been validated for several zeolitic systems.[3d,16a] For the fitting procedure of the obtained NMRD data, the following limitations and constraints were applied. The distance r_{GdH} was fixed at 3.1 Å, E_v at 1 kJ mol^{-1}, q at the values obtained from the luminescence decay experiments ($q = 1$ and 6 for the extracted and loaded sample, respectively), and w at the values calculated from the known total amount of water in the zeolites and from the Gd loading.[20] Furthermore, the correlation times τ_m and τ_{zeo} were limited by the boundaries discussed in the manuscript. Attempts to fit the data with correlation times outside these boundaries led to unsatisfactory fits and/or to unrealistic values for the variable parameters, such as negative activation energies. It may be expected that τ_{zeo} is the same for calcined and uncalcined Gd-LTL and it should be smaller than 10^{-7} s. Since Figure 5 C shows that under these conditions τ_{zeo} has almost no influence on r_1, its value was fixed at 10^{-8} s. Finally, we have included in the fittings some values of transverse electronic rates ($1/T_{2e}$) as obtained from EPR peak-to-peak line widths (Figure S4 in the Supporting Information) with Equation (6), in which μ_B is the Bohr

magneton, g_L the electron Landé factor, h the Planck constant, and ΔH_{pp} the peak-to-peak line width.

$$\frac{1}{T_{2e}} = \frac{g_L \mu_B I \Pi \sqrt{3}}{\eta} \Delta H_{pp} \quad (6)$$

Although the number of variables was still substantial, the obtained best-fit values turned out to be reasonable. They are compiled in Table 1 and NMRD profiles calculated with these values are represented as curves in Figure 5 B. For comparison, some previously determined data on Gd^{III}-loaded zeolite NaY and mesoporous material AlTUD-1 are included in Table 1. The best-fit values of the parameters governing the transversal electronic relaxation rates, τ_v and Δ^2, are in the range usually observed for Gd^{III} loaded zeolites.[3d,14,16] The values of $1/T_{2e}$, measured by EPR at 0.34 T (9.77 G) are in a good agreement with the best-fit values (see Table 1). The values for τ_m are very small compared to that of Gd-NaY with a comparable loading. In Gd-NaY systems, the water exchange process in the zeolite supercages speeds up substantially upon increasing the Gd^{III} loading, which is a consequence of the increase of the Gd^{III} concentration inside the zeolite cavities, which makes the probability of a water molecule being located in the inner coordination sphere of the Gd^{III} ion higher. In the studied Gd-LTL-L system presented here, the residence time of water inside the zeolite (τ_{zeo}) is so short that in this case the exchange process is probably not limited to the water inside the zeolite nanoparticles. For the Gd-LTL-E sample, however, the value for τ_m is rather large, which may be rationalized by the locked location of the Gd^{III} ions after calcination. Assuming that the exchange follows a dissociative mechanism, the encapsulation may lead to a relatively high steric strain on the remaining bound water molecule and, consequently, lead to a relatively large free enthalpy gap between the ground state and the eight-coordinate transition state and thus to a relatively slow water exchange rate.

Acknowledgements

This research was performed in the framework of the EU COST Action TD1004, "Theranostics Imaging and Therapy: an Action to Develop Novel Nanosized Systems for Imaging-Guided Drug Delivery" and supported by: the Dutch Ministry of Economy of the Province of Zuid-Holland (F.M., the 3Binding project "Imaging, Interpretation and Therapy; Innovation in Nuclear Diagnostics and Therapy Health Care"), China Scholarship Council (W.Z.), and the Netherlands Organization for Scientific Research (K.D., NWO Veni grant 722.012.009). The authors thank Prof. W. R. Hagen (TU Delft) for the EPR measurements, F. Szeremeta and S. Même (CNRS, Orléans, FR) for the MR images, and Dr. H. S. Figueiredo and Prof. I. Correia Neves (Braga, PT) for exploratory experiments.

Keywords: bimodal imaging · ion relocation · lanthanides · luminescence · relaxivity · zeolites

[1] a) J. Čejka, H. van Bekkum, A. Corma, F. Schueth in *Introduction to Zeolite Science and Practice*, Elsevier, Amsterdam (The Netherlands), **2007**; b) H. van Bekkum, H. W. Kouwenhoven in *Zeolite Manual for the Organic Chemist*, Mijnbestseller.nl, **2012**; c) XRD profiles of Linde Type L framework are available at http://www.iza-online.org/, **2014**.
[2] J. Scherzer, *Catal. Rev. Sci. Eng.* **1989**, *31*, 215.
[3] a) K. J. Balkus, D. A. Sherry, S. W. Young, (The University of Texas System, USA), US5122363, **1992**; b) D. L. Rubin, K. L. Falk, M. J. Sperling, M. Ross, S. Saini, B. Rothman, F. Shellock, E. Zerhouni, D. Stark, E. K. Outwater, U. Schmiedl, L. C. Kirby, J. Chezmar, T. Coates, M. Chang, J. M. Silverman, N. Rofsky, K. Burnett, J. Engel, S. W. J. Young, *Magn. Reson. Imaging* **1997**, *7*, 865; c) S. W. Young, F. Qing, D. Rubin, K. J. Balkus, J. S. Engel, J. Lang, W. C. Dow, J. D. Mutch, R. A. Miller, *Magn. Reson. Imaging* **1995**, *5*, 499; d) É. Csajbók, I. Bányai, L. Vander Elst, R. N. Muller, W. Zhou, J. A. Peters, *Chem. Eur. J.* **2005**, *11*, 4799; e) J. A. Peters, K. Djanashvili, *Eur. J. Inorg. Chem.* **2012**, 1961.
[4] S. Aime, C. Cabella, S. Colombatto, S. Geninatti Crich, E. Gianolio, F. J. Maggioni, *Magn. Reson. Imaging* **2002**, *16*, 394.
[5] P. A. Newell, L. V. C. Rees, *Zeolites* **1983**, *3*, 22.
[6] L. Frullano, T. J. Meade, *J. Biol. Inorg. Chem.* **2007**, *12*, 939.
[7] R. M. Barrer, J. Villinger, *Z. Kristallgr.* **1969**, *128*, 352.
[8] J.-C. G. Bünzli, *Chem. Rev.* **2010**, *110*, 2729.
[9] a) A. E. Merbach, L. Helm, É. Tóth in *The Chemistry of Contrast Agents in Medical Magnetic Resonance Imaging*, 2nd ed. (Eds.: A. E. Merbach, É. Tóth), John Wiley & Sons, Chichester, **2013**, pp. 25–81; b) P. Caravan, J. J. Ellison, T. J. McMurry, R. B. Lauffer, *Chem. Rev.* **1999**, 2293.
[10] D. M. Corsi, C. Platas-Iglesias, H. van Bekkum, J. A. Peters, *Magn. Reson. Chem.* **2001**, *39*, 723.
[11] W. D. Horrocks, D. R. Sudnick, *J. Am. Chem. Soc.* **1979**, *101*, 334.
[12] P. Gillis, S. Peto, R. N. Muller, *Magn. Reson. Imaging* **1991**, *9*, 703.
[13] a) V. Kubíček, J. Rudovský, J. Kotek, P. Hermann, L. Vander Elst, R. N. Muller, Z. I. Kolar, H. T. Wolterbeek, J. A. Peters, I. Lukeš, *J. Am. Chem. Soc.* **2005**, *127*, 16477; b) I. Rehor, V. Kubicek, J. Kotek, P. Hermann, I. Lukes, J. Szakova, L. Vander Elst, R. N. Muller, J. A. Peters, *J. Mater. Chem.* **2009**, *19*, 1494; c) T. Vitha, V. Kubíček, P. Hermann, L. Vander Elst, R. N. Muller, Z. I. Kolar, H. T. Wolterbeek, W. A. P. Breeman, I. Lukeš, J. A. Peters, *J. Med. Chem.* **2008**, *51*, 677.
[14] C. Platas-Iglesias, L. Vander Elst, W. Zhou, R. N. Muller, C. F. G. C. Geraldes, T. Maschmeyer, J. A. Peters, *Chem. Eur. J.* **2002**, *8*, 5121.
[15] J. Caro, S. Hőcevar, J. Kärger, L. Riekert, *Zeolites* **1986**, *6*, 213.
[16] a) M. Norek, I. C. Neves, J. A. Peters, *Inorg. Chem.* **2007**, *46*, 6190; b) N. M. K. Tse, D. F. Kennedy, N. Kirby, B. A. Moffat, B. W. Muir, R. A. Caruso, C. Drummond, *J. Adv. Healthcare Mater.* **2013**, *2*, 836.
[17] a) S. P. Hudson, R. F. Padera, R. Langer, D. S. Kohane, *Biomaterials* **2008**, *29*, 4045–4055; b) R. S. Bedi, D. E. Beving, L. P. Zanello, Y. Yan, *Acta. Biomater.* **2009**, *5*, 3265–3271.
[18] A. Barge, G. Cravotto, E. Gianolio, F. Fedeli, *Contrast Media Mol. Imaging* **2006**, *1*, 184.
[19] a) N. Bloembergen, L. O. Morgan, *J. Chem. Phys.* **1961**, *34*, 9; b) I. Solomon, *Phys. Rev.* **1955**, *99*, 559.
[20] The w value was calculated from the molecular formula of the zeolite $K_6Na_3(H_2O)_{21}Al_9Si_{27}O_{72}$ in combination with the loading. In detail, an average of one Gd^{III} ion per unit cell was loaded into the framework. 21 water molecules are present per unit cell of which 15 are free and 6 are coordinated to the Gd-center ($q = 6$).

Received: November 14, 2013
Published online on February 12, 2014

